COMPUTATIONAL STUDIES OF AEROELASTICITY OF AIRCRAFT ENGINE TURBINE BLADE

Marcel ILIE[1], Augustin SEMENESCU[2]

Rezumat. *Modul tranzitoriu al sarcinii aerodinamice a unei palete de turbină a unui motor de avion reduce timpul de viață al paletei și, ca urmare, timpul de viață al motorului. De aceea, o estimare corectă a sarcinii aerodinamice și un model cuplat al aerodinamicii și structurii poate crește timpul de viață al paletei turbinei și a motorului, prin reducerea timpilor de întreținere. Această cercetare investighează instabilitatea vibrațiilor paletei de turbine a unui motor de avion, în condiții de instabilitate aerodinamică. Ecuațiile Navier-Stokes împreună cu modelul SST-kω pentru turbulență sunt rezolvate pe cale numerică. Studiul arată faptul că vibrațiile produc variații temporale ale coeficienților aerodinamici.*

Abstract. *Transient blade loading limits the lifetime of aircraft engine turbine blades. Thus, accurate prediction of the unsteady aerodynamic loading and coupled fluid-structure interactions would improve the life the lifetime of the turbine blades. This study investigates the flutter instability of an axial turbine blade under unsteady aerodynamic loading. The viscous Navier-Stokes equations with the SST-kω turbulence model are employed. The results show that the flutter phenomenon causes unsteady oscillations of the aerodynamic coefficients lift and drag.*

1. Introduction

Aeroelasticity is an important and critical phenomenon encounter in many aerospace applications such as airplane wing, compressor/turbine blades, helicopter blades, etc. In gas turbine engine, the aeroelasticity is a major concern due to the fact that it decreases the engine performance and poses critical issues. The flutter phenomenon causes fatigue failure of the blade and therefore, it poses

---

[1]PhD, Assistant Professor: Dept. of Mechanical Engineering, Georgia Southern University, Statesboro, GA 30458, USA. E-mail: milie@georgiasouthern.edu
[2]PhD, Professor, Dept. of Material Sciences, University Politehnica Bucharest, Bucharest, Romania; Associate Member of Academy of Romanian Scientists. E-mail: augustin.semenescu@upb.ro

significant safety challenges. The flutter phenomenon leads to the early material fatigue and usually, it results in the cracking of the blade material. Due to the rotational nature of the turbine stage, the material fracture of one blade leads to the destruction of the entire turbine stage. This is due to the very small clearance between the tip of the blade and casing. One way to mitigate the fatigue would be the use of high-density materials. However, the use of these materials increases the overall weight of the engine and thus, the fuel consumption and implicitly the overall cost of the flight/mission. Therefore, the prediction of the flutter phenomenon would benefit significantly the life span of the engine and increase the aircraft performance and engine safety.

Experimental studies of aeroelasticity are challenging due to the fact that involve the use of intrusive methods and instrumentation. Thus, the computational methods are a promising alternative
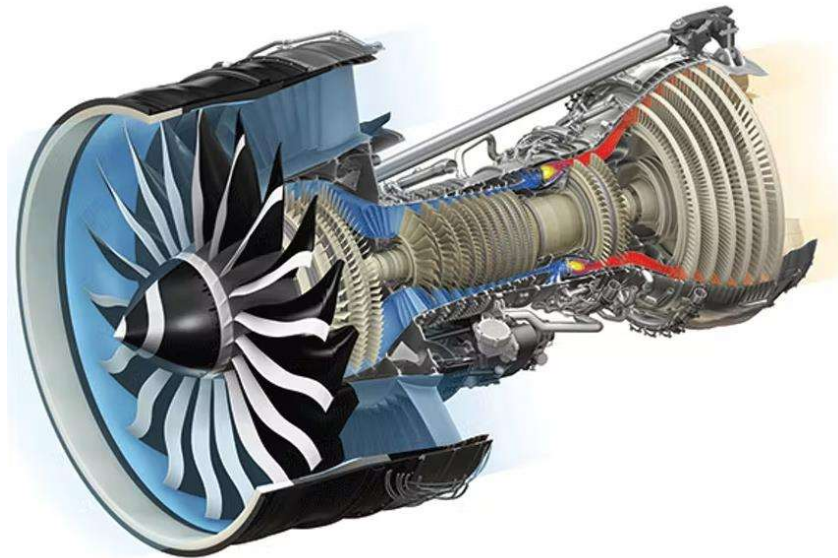
Fig. 1. Scheme of fuel injection for scramjet combustion [14]

Figure 1 presents the schematic of the aircraft engine. The flutter phenomenon is due to the interaction between the incoming air and blades. The fluid-structure interaction phenomenon "poses significant challenges due to the complex fluid dynamics such as horseshoe vortices, jet shear-layer and wake vortices" (see the Figure 2) [2]. These flow structures impact the fluid-structure phenomenon in a particular way and the understanding of their development and evolution would enable a better understanding of the flutter phenomenon. The study of flutter phenomenon requires the use of fully-coupled fluid-structure computational approaches. Therefore, one of the main objectives of the present research is the

development of a fully-coupled fluid-structure approach for the study of flutter phenomenon of aircraft engine turbine blade.
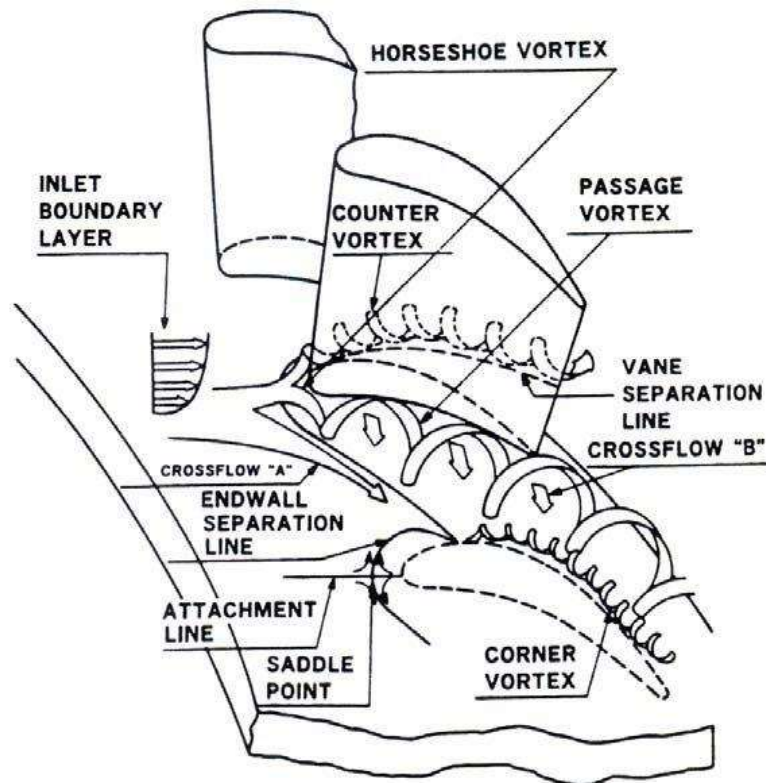

Fig. 2. Cavity flow for supersonic combustion [13]

2. Background of computational method

Computational methods have been made in the past in the computation of fluid-structure interaction phenomenon. The first methods employed the vortex panel methods [3]. However, these methods assume that the flow is inviscid and therefore, it cannot capture the flow separation and predict the drag coefficient. Therefore, viscous methods must be employed in the computation of high Reynolds number flows [2]…[20]. Studies showed that the numerical approach based on the "Reynolds-averaged Navier-Stokes (RANS) are not suitable for time-dependent flow dynamics such as the unsteady aerodynamics of compressor/turbine stage" [15]. Direct numerical simulations (DNS) also pose computational challenges due to the high-resolution grid size required by the DNS. Generally, DNS approach "is not suitable for high Reynolds number flows and thus, alternative time-dependent solutions must be sought. Therefore, large-

eddy simulation (LES) approach is a promising approach for the numerical computations of high-Reynolds number flows in a rotating-frame of reference" [15].

3. Modeling

As already mentioned in this research we will employ the LES approach. The equations of LES approach model are the filtered Navier-Stokes equations (1) and (2)

$$\frac{\partial \overline{u}_i}{\partial x_i} = 0 \tag{7}$$

$$\frac{\partial \overline{u}_i}{\partial t} + \frac{\partial}{\partial x_j}\left(\overline{u}_i \overline{u}_j\right) = -\frac{\partial \overline{p}}{\partial x_i} - \frac{\partial \tau_{ij}}{\partial x_j} + \frac{1}{R_e}\frac{\partial^2 \overline{u}_i}{\partial x_j \partial_j} \tag{8}$$

where

$$\tau_{ij} = \overline{u_i u_j} - \overline{u}_i \overline{u}_j \tag{9}$$

The LES approach was used in the authors' previos studies [15]. "The SGS Reynolds stress, (τ_{ij}), is similar to the Reynolds stress in RANS in the sense that in both cases the unresolved scales (u') (small eddies in LES and turbulent fluctuations in RANS) are regarded as producing stresses in the resolved scales (large eddies in LES and mean velocity in RANS). The difference is that in RANS, (u') represents all the turbulent motions, while in LES (u') represents only the small eddies or sub-grid scales. This means that the energy in the unresolved scales of LES (sub-grid scales) represents a much smaller fraction of the total flow energy compared to the energy in the unresolved scales of RANS (the turbulent fluctuations)" [15].

In general,

$$\overline{u_i u_j} \neq \overline{u}_i \overline{u}_j$$

(10)

and therefore, Reynolds stress tensor (τ_{ij}) has to be modeled. The sub-grid scale (SGS) tensor τ_{ij} is expressed as:

$$\tau_{ij} - \frac{1}{3}\tau_{kk}\delta_{ij} = 2\nu \overline{S}_{ij}$$

(11)

where $\overline{S}_{ij}$ is the strain rate based on the filtered velocity $\overline{u}_i$ and the eddy-viscosity ν

$$\overline{S}_{ij} = \frac{1}{2}\left(\frac{\partial \overline{u}_i}{\partial x_j} + \frac{\partial \overline{u}_j}{\partial x_i} \right)$$

(12)

Smagorinsky model is an algebraic model for the subgrid scale (SGS) viscosity ν_{sgs}.

The space and time-discretization are presented in the following and were used in the authors' previous studies [15]. Figure 1 shows "the time and space-marching schemes with space on the horizontal and time on the vertical. For simplicity, an equally spaced computational domain will be used, with the space and time variables h and t. As shown in Figure 5, for the space marching of the solution, the time is fixed and solution is computed at the computational grid points $f(t, x - h)$, $f(t, x)$ and $f(t, x + h)$".
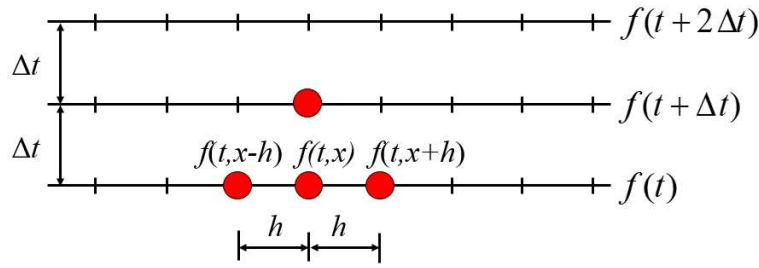

Fig. 3. Space and time-discretization

Figure 6 shows "the time-discretization of the Laplace equation. For the time-marching, the space is kept constant while the time increment is $t + \Delta t$" [20].
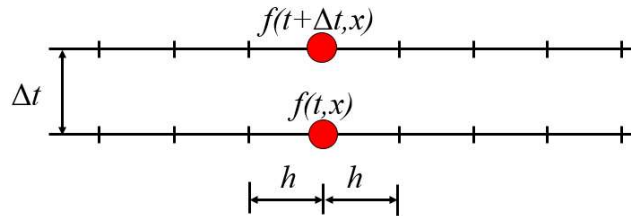

Fig. 4. Time-discretization

"The finite-difference approach makes use of the Taylor series. Thus, the Taylor series is sued for an arbitrary function f, where f can represent the flow variables such as pressure or velocity" [20]. The Taylor series expanded about the grid point $(x + h)$ becomes

$$f(x+h) = f(x) + \frac{\partial f(x)}{\partial x}h + \frac{\partial^2 f(x)}{\partial x^2}\frac{h^2}{2} + \frac{\partial^3 f(x)}{\partial x^3}\frac{h^3}{6} + \frac{\partial^4 f(x)}{\partial x^4}\frac{h^4}{24} + ...$$

$$f(x-h) = f(x) - \frac{\partial f(x)}{\partial x}h + \frac{\partial^2 f(x)}{\partial x^2}\frac{h^2}{2} - \frac{\partial^3 f(x)}{\partial x^3}\frac{h^3}{6} + \frac{\partial^4 f(x)}{\partial x^4}\frac{h^4}{24} + ...$$

By subtracting equation 3 from equation 2 and canceling the high-order terms, the difference $f(x+h) - f(x-h)$ is obtained in the following form:

$$4. \quad f(x+h) - f(x-h) = 2\frac{\partial f(x)}{\partial x}h + 2\frac{\partial^3 f(x)}{\partial x^3}\frac{h^3}{6} + ...$$

Rearranging this equation to isolate the first derivative, we obtain the following equation:

$$5. \quad \frac{\partial f(x)}{\partial x} = \frac{f(x+h) - f(x-h)}{2h} - \frac{\partial^3 f(x)}{\partial x^3}\frac{h^2}{6}$$

Next, we need to find the second derivative of function f. Making use again of the Taylor series:

$$f(x+h) = f(x) + \frac{\partial f(x)}{\partial x}h + \frac{\partial^2 f(x)}{\partial x^2}\frac{h^2}{2} + \frac{\partial^3 f(x)}{\partial x^3}\frac{h^3}{6} + \frac{\partial^4 f(x)}{\partial x^4}\frac{h^4}{24} + ...$$

$$f(x-h) = f(x) - \frac{\partial f(x)}{\partial x}h + \frac{\partial^2 f(x)}{\partial x^2}\frac{h^2}{2} - \frac{\partial^3 f(x)}{\partial x^3}\frac{h^3}{6} + \frac{\partial^4 f(x)}{\partial x^4}\frac{h^4}{24} + ...$$

$$6.$$

Adding equations, we obtain:

$$7. \quad f(x+h) + f(x-h) = 2f(x) + 2\frac{\partial f^2(x)}{\partial x^2}\frac{h}{2} + 2\frac{\partial^4 f(x)}{\partial x^4}\frac{h^4}{24} + ...$$

Rewriting this equation in order to isolate the second derivative, we obtain the second derivative of function f in the form:

$$\frac{\partial^2 f(x)}{\partial x^2} = \frac{f(x+h) - 2f(x) + f(x-h)}{h^2} - \frac{\partial^4 f(x)}{\partial x^4}\frac{h^2}{12} + ...$$

Eliminating the high-order terms the second derivative becomes:

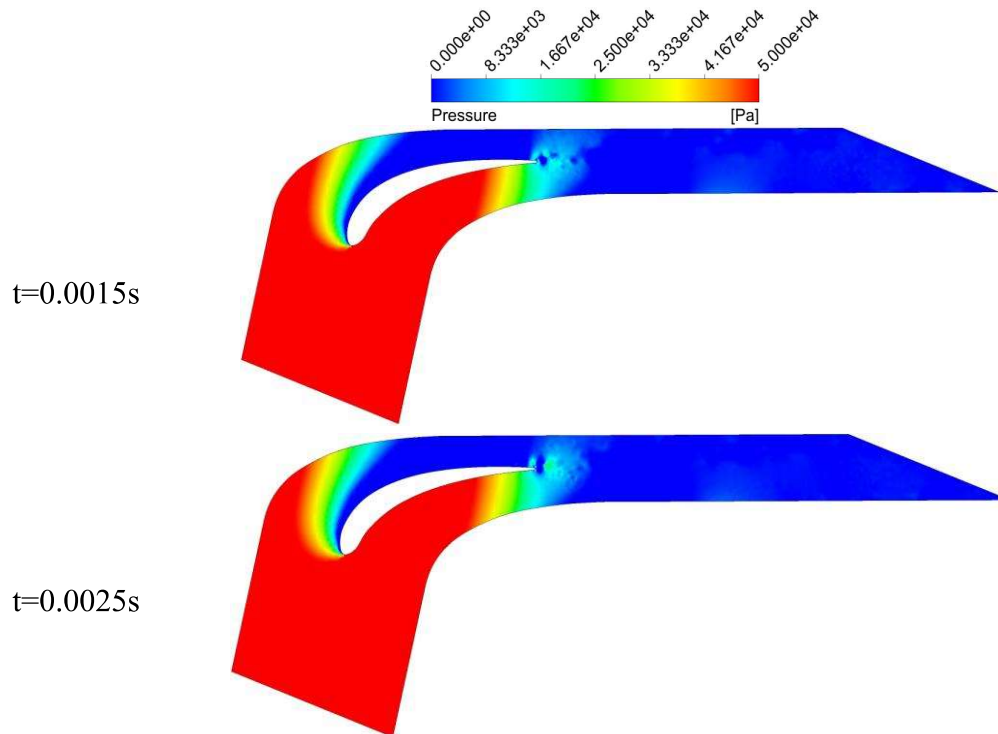$$\frac{\partial^2 f(x)}{\partial x^2} = \frac{f(x+h) - 2f(x) + f(x-h)}{h^2}$$

8.   Results and discussion

Figure 5 presents the velocity field for the turbine blade. The analysis of the velocity field reveals that there is an increase of the velocity on the suction side of the blade, while the pressure side undergoes lower velocity. The high-speed flow generates large turbulent scales at the trailing-edge of the blade.
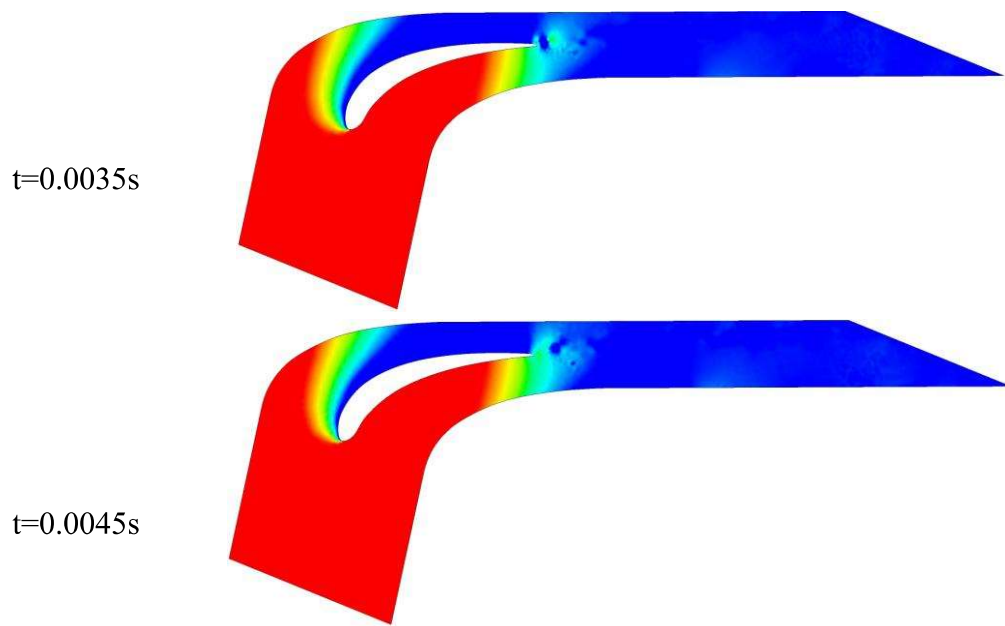
t=0.0015s

t=0.0025s

t=0.0035s

t=0.0045s

Fig. 5 . Velocity field
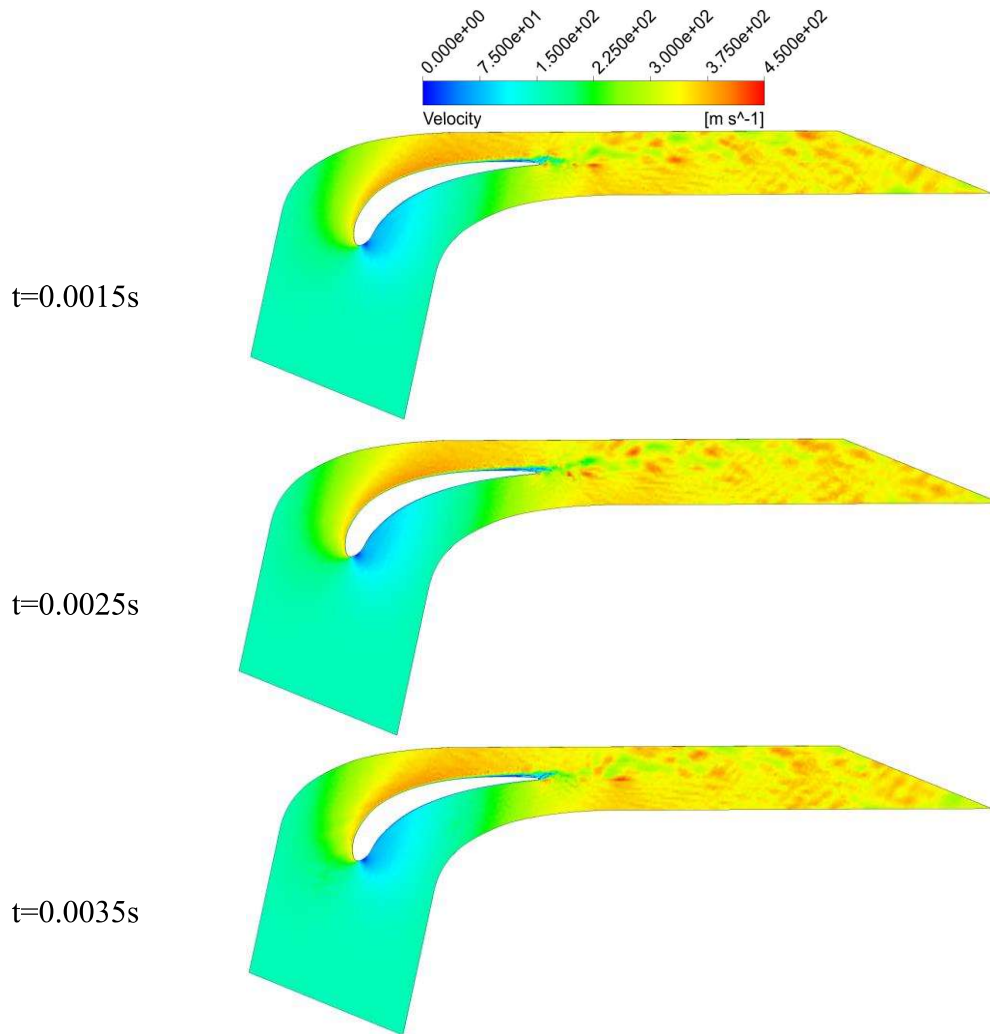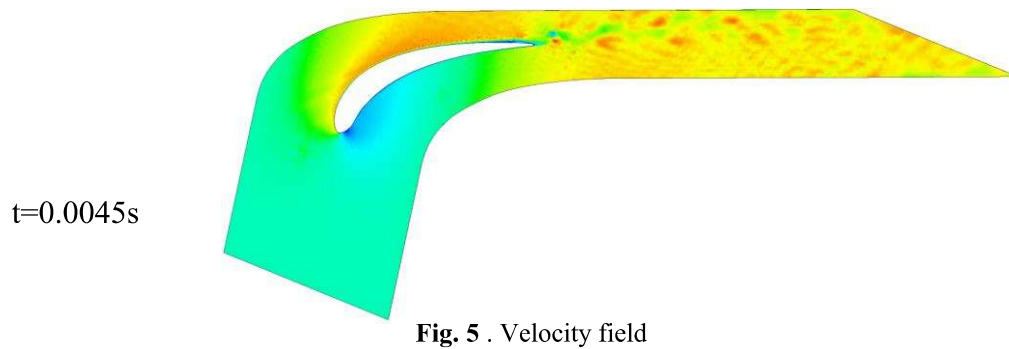
It is expected that the turbulence present at the trialing-edge of the blade would cause vibrations of the blade and therefore, further damage of the blade structure. As shown in Figure 5, it can be seen that the turbulence does not decay with time and it rather amplifies. The turbulence fluctuations are reflected in the pressure field as well and this is shown in Figure 6. As seen in Figure 6, the pressure is high on the pressure side of the blade and exhibits lower levels on the suction side. Similar to the velocity field, the pressure also exhibits fluctuations at the trialing-edge and these fluctuations would affect the flutter phenomenon. Due to the turbulence levels, the Reynolds stress also shows large values, as shown in Figure 7.
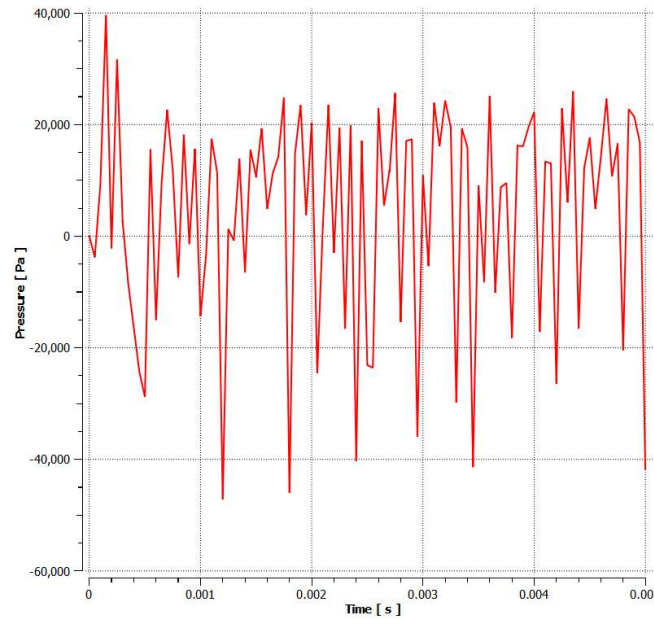

t=0.0015s

t=0.0025s

t=0.0035s

t=0.0045s

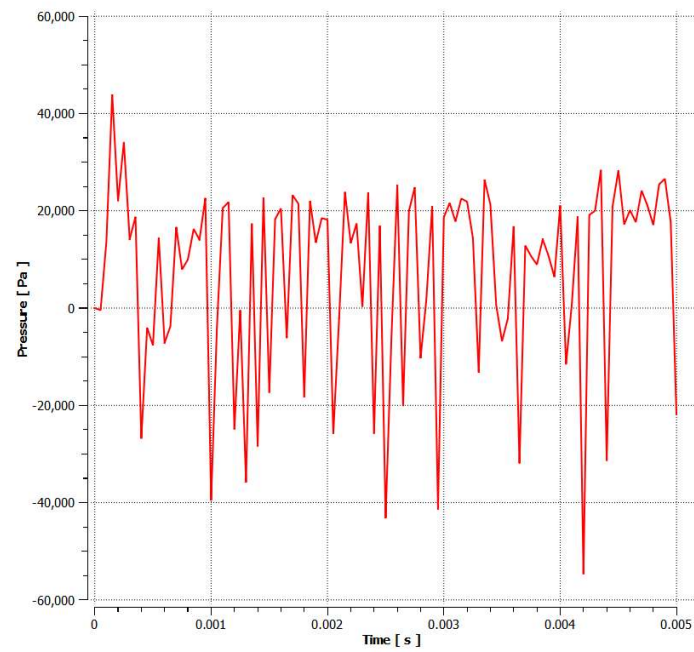**Fig. 6.** Pressure field

t=0.0015s

t=0.0025s

t=0.0035s

t=0.0045s
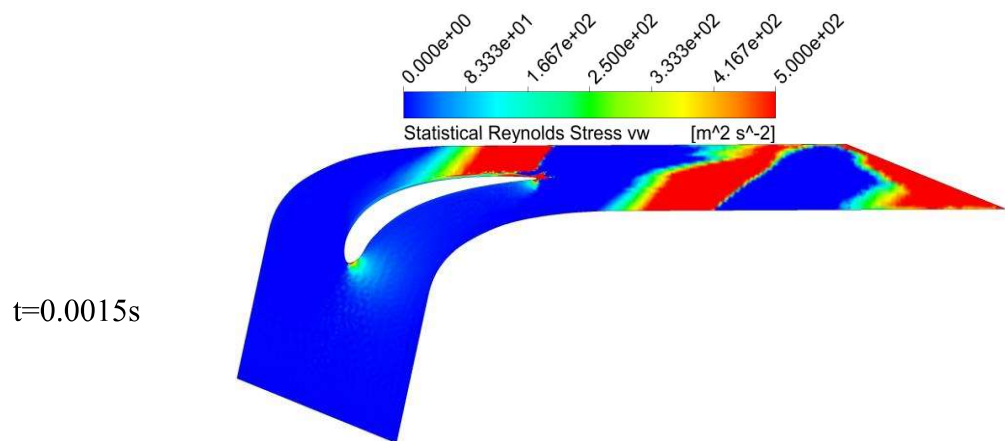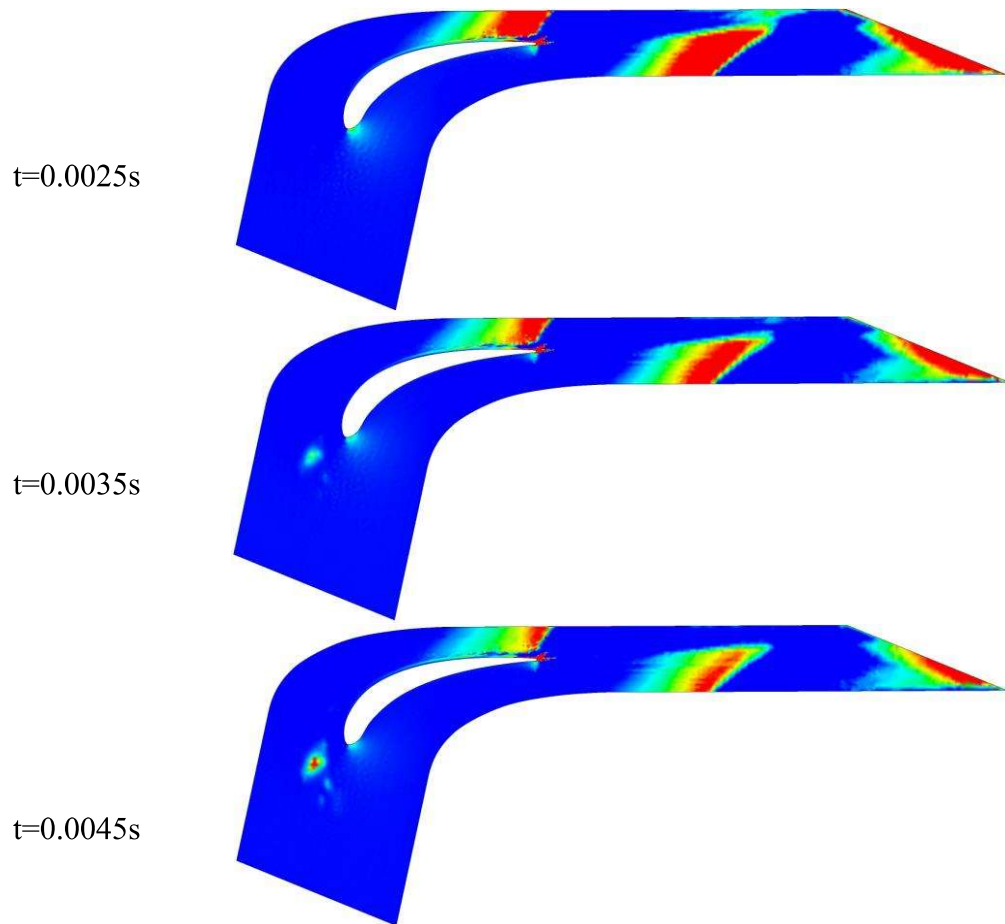
Fig. 7. Reynolds stresses

Fig. 8. Pressure field

Figure 8 presents the time-varying pressure at the trialing-edge of the blade. The analysis of the pressure field shows that the pressure field undergoes significant fluctuations. Figure 8 presents the pressure at a location in the region of the suction side of the blade. Figure 9 presents the pressure fluctuations at location also in the suction region of the blade. Figure 9 presents the pressure field in the region of the suction side. The analysis of the pressure field shows that there are large fluctuations of the pressure and it is expected that this would have impact on the flutter phenomenon. Figure 11 presents the pressure fluctuations on the suction side of the blade. However, away from the blade these pressure fluctuations decrease and this is shown in Figure 11.
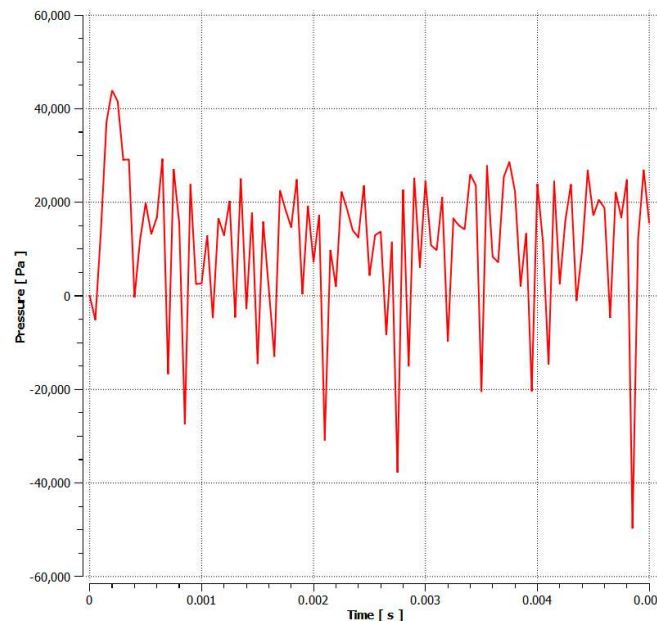
Fig. 9. Pressure field
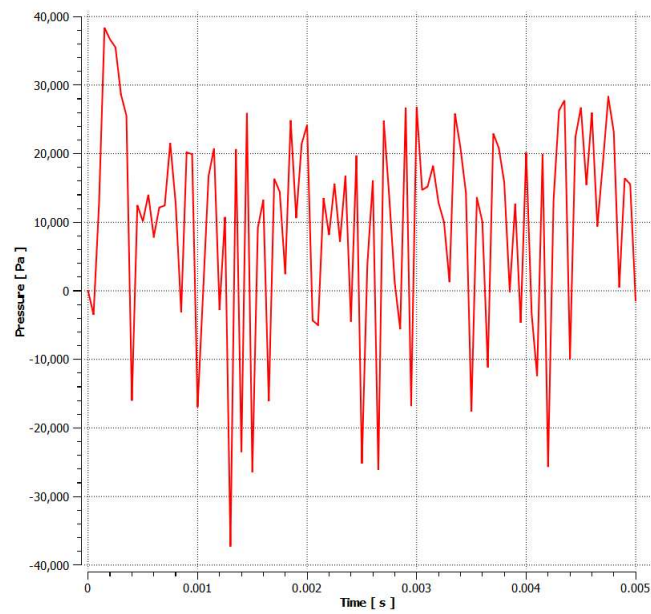
Fig. 10. Pressure field

Fig. 11. Pressure field

Conclusions

An efficient computational approach, for the fluid-structure interaction, is obtained for the case of large Reynolds number flows. The current model is employed for the computation of aeroelasticity effects in highly turbulent flows. The analysis of the flutter phenomenon shows that the pressure fluctuation increase the flutter phenomenon and it increases with the Reynolds number. The study also shows that there is a strong interaction between the vortices developed at the trailing-edge of the stator blade and the leading-edge of the rotor blade row. The frequency of the vortex shedding governs the blade-vortex interactions. Thus, the higher the vortex shedding frequency, the higher the vibrations of the rotor blades.

R E F E R E N C E S

[1] Urzay, J., Supersonic Combustion in Air-Breathing Propulsion Systems for Hypersonic Flight, Annual Review of Fluid Mechanics, 50:1, 593-627, 2018

[2] Karagozian, A. R., 2010, Transverse Jets and Their Control, Prog. Energy Combust. Sci., 36(5), pp. 531–553, 2010

[3] Mahesh, K., 2012, The Interaction of Jets With Crossflow, Annu. Rev. Fluid Mech., 45(1), pp. 379–407, 2012

[4] Karagozian, A. R., 2014, The Jet in Crossflow," Phys. Fluids, 26(3), pp. 1–17.

[5] Fric, T. F., and Roshko, A., Vortical Structure in the Wake of a Trans- verse Jet," J. Fluid Mech., 279, pp. 1–47, 1994

[6] New, T.H., Lim, T.T. & Luo, S.C. Effects of jet velocity profiles on a round jet in cross-flow. Exp Fluids 40, 859–875, 2006

[7] Kelso, R. M., Lim, T. T., and Perry, A. E., An Experimental Study of Round Jets in Cross-Flow, J. Fluid Mech., 306, pp. 111–144, 1996

[8] Su, L. K., and Mungal, M. G., Simultaneous Measurements of Scalar and Velocity Field Evolution in Turbulent Crossflowing Jets, J. Fluid Mech., 513, pp. 1–45, 2004

[9] Gopalan, S., Abraham, B. M., and Katz, J., The Structure of a Jet in Cross Flow at Low Velocity Ratios," Phys. Fluids, 16(6), 2067–2087, 2004

[10] Shan, J. W., and Dimotakis, P. E., Reynolds-Number Effects and Anisotropy in Transverse-Jet Mixing, J. Fluid Mech., 566, pp. 47–96, 2006

[11] Galeazzo, F. C. C., Donnert, G., Habisreuther, P., Zarzalis, N., Valdes, R. J., and Krebs, W., Measurement and Simulation of Turbulent Mixing in a Jet in Crossflow, ASME J. Eng. Gas Turbines Power, 133(6), p. 061504, 2011

[12] Muppidi, S., and Mahesh, K., Study of Trajectories of Jets in Crossflow Using Direct Numerical Simulations," J. Fluid Mech., 530, pp. 81–100, 2005

[13] Takeishi, K., M. Matsuura, S. Aoki, and T. Sato (1990). An experimental study of heat transfer and film cooling on low aspect ratio turbine nozzles. J. of Turbomach. 112, 488—496.

[14]   https://www.machinedesign.com/motors-drives/article/21832035/whats-the-difference-between-turbine-engines

[15] M. Ilie, A. Semenescu, G. Liliana Stroe, S. Berbente, Numerical Computations of the cavity flow using the potential flow theory, Annals of the Academy of Romanian Scientists Series on Engineering Sciences, Volume 13, Number 2/2021, ISSN 2066-8570

[16] M. Ilie. "A computational model for cardiovascular hemodynamics and protein transport phenomena", Health and Technology, 2021

[17] M. Ilie, Augustin Semenescu, Matthew Chan. "Computational studies of turbine- stage, with variable inlet temperature; comparison between LES and IDDES", AIAA AVIATION 2021 FORUM, 2021

[18] M. Ilie, Matthew Chan, Jackson Asiatico. "Combustion instabilities in backward-step premixed reacting flows; computational studies using LES", AIAA SCITECH 2022 Forum, 2022